J. Appl. Comput. Mech., xx(x) (2026) 1-13
DOI: 10.22055/jacm.2026.49286.5867

ISSN: 2383-4536
jacm.scu.ac.ir

Shahid Chamran University of Ahvaz

Journal of Applied and Computational Mechanics

Research Paper

ANFIS-Based Modeling and Optimization of Heat Transfer in Ultrasonically Assisted Finned-Tube Heat Exchangers with MWCNT Nanofluids

Amin Amiri Delouei

Department of Mechanical Engineering, University of Bojnord, Bojnord, Iran, Email: a.amiri@ub.ac.ir

Received April 23 2026; Revised June 10 2026; Accepted for publication June 11 2026.
✉ Corresponding author: A. Amiri Delouei (a.amiri@ub.ac.ir)

Abstract. This study examines the thermal performance of a finned-tube heat exchanger enhanced with multi-walled carbon nanotube (MWCNT) nanofluids under ultrasonic excitation. An experimental setup is designed to evaluate the effects of inlet temperature, air velocity, nanoparticle concentration, and ultrasonic power on outlet temperature, heat transfer rate, and Nusselt number. An adaptive neuro-fuzzy inference system (ANFIS) is developed to represent the nonlinear behavior of the system. Model parameters are optimized using a genetic algorithm (GA) and particle swarm optimization (PSO). A dataset of 108 experimental samples is used, with 81 samples allocated for training and 27 samples allocated for testing. The predictions show strong agreement with experimental data, with coefficients of determination up to 0.98. The ANFIS–GA model achieves lower prediction errors and more consistent performance than ANFIS–PSO. Sensitivity analysis identifies the inlet temperature, nanoparticle concentration, and ultrasonic power as the dominant parameters, whereas the air velocity has a weaker effect. The results confirm that ultrasonic excitation combined with nanofluids improves heat transfer performance. The proposed ANFIS–GA framework provides an accurate and efficient alternative to extensive experimental testing.

Keywords: Finned-tube heat exchanger, Ultrasonic vibration, Nanofluid, ANFIS–GA, ANFIS–PSO.

1. Introduction

The efficient design and operation of heat exchangers are essential for a wide range of industrial applications, including energy systems [1], chemical processing [2], and thermal management [3]. Optimization techniques such as Genetic Algorithm (GA), Particle Swarm Optimization (PSO), and Response Surface Methodology (RSM) have been extensively applied to improve heat transfer performance and reduce energy consumption in thermal systems [4–6]. These methods enable systematic tuning of operating parameters and facilitate the identification of optimal conditions.

In recent years, intelligent data-driven methods have received considerable attention for modeling and optimization of heat exchangers. These methods are capable of capturing complex nonlinear relationships between operating parameters. Among them, the Adaptive Neuro-Fuzzy Inference System (ANFIS) has emerged as a powerful and reliable tool for predicting thermal and fluid flow behavior. For instance, ANFIS has been effectively implemented in helicoidal double-pipe heat exchangers, where it has shown strong predictive capability for estimating the total heat transfer coefficient and pressure drop using relevant dimensionless parameters [7]. Similarly, its application in shell-and-tube heat exchangers has shown superior predictive performance compared to conventional artificial neural networks, particularly in nonlinear systems [8].

Recent studies have further confirmed the effectiveness of ANFIS in modeling complex thermal processes. An ANFIS-based model was developed to predict frost formation in finned-tube heat exchangers (FTHXs) using extensive experimental data, achieving very high correlation coefficients [9]. In another study, ANFIS was applied to estimate the heat transfer coefficient in shell-and-tube heat exchangers, resulting in improved accuracy compared to traditional approaches [10]. Moreover, comparative analyses between ANFIS and ANN in shell-and-tube heat exchangers indicated that ANFIS provides more reliable predictions, especially for limited datasets and highly nonlinear interactions [10]. In parallel, evolutionary optimization algorithms such as GA and PSO have been widely used to enhance thermal system performance. For instance, GA has been integrated with first-principles models to optimize operating conditions in plate-fin heat exchangers, leading to enhanced thermal effectiveness and reduced computational cost [11]. In addition, hybrid ANFIS-PSO models have been developed to predict key performance indicators, including heat transfer rate and Nusselt number, with high accuracy and strong agreement with experimental data [6]. Other data-driven methods, such as RSM and Group Method of Data Handling (GMDH), have also demonstrated high predictive capability under ultrasonic conditions [5]. Taken together, existing studies indicate that the integration of intelligent modeling approaches with evolutionary optimization algorithms can markedly enhance predictive accuracy and overall system performance.

Published online: June 18 2026

In recent years, the use of nanofluids and ultrasonic enhancement techniques has emerged as an effective approach to improve heat transfer performance [12]. Nanofluids, which consist of base fluids with suspended nanoparticles, can significantly enhance thermal conductivity and convective heat transfer [13, 14]. At the same time, ultrasonic waves improve fluid mixing and reduce thermal boundary layer resistance, leading to further enhancement in heat transfer efficiency [15–17]. Recent experimental investigations have explored the combined effects of nanofluids and ultrasonic excitation in heat [18, 19].

Despite these advances, limited research has focused on the application of intelligent modeling techniques to ultrasonically assisted FTHXs operating with nanofluids. Previous studies have primarily examined the thermal effects of nanofluids and ultrasonic excitation through experimental investigations or have applied ANFIS-based models to other heat transfer systems. To the best of the authors' knowledge, ANFIS-GA and ANFIS-PSO models have not previously been applied to predict the thermal performance of an ultrasonically assisted FTHX using MWCNT nanofluids.

In the present study, an ANFIS model is developed to predict the heat transfer performance of a FTHX enhanced with MWCNT nanofluids under ultrasonic excitation. The model captures nonlinear interactions between inlet temperature, air velocity, nanoparticle concentration, and ultrasonic power. The output variables include outlet temperature, heat transfer rate, and Nusselt number, which represent key performance indicators of the system. To further improve prediction accuracy, ANFIS parameters, including membership functions and rule coefficients, are optimized using GA [20, 21] and PSO [20–22]. The developed approach reduces the need for extensive experimental measurements by enabling accurate prediction of unmeasured conditions. The model is developed using a dataset of 108 experimental samples, with nearly 75% allocated to the training phase and the remaining portion used for testing. This data division ensures reliable model validation and robustness. The novelty of the present study lies in the development of ANFIS-GA and ANFIS-PSO models based on experimental data obtained from an ultrasonically excited FTHX. The GA and PSO algorithms are employed to optimize the ANFIS model parameters and improve prediction accuracy. The predictive performances of the two approaches are systematically compared using outlet temperature, heat transfer rate, and Nusselt number as target variables. In addition, a sensitivity analysis is performed to quantify the relative influence of inlet temperature, air velocity, ultrasonic power, and nanofluid concentration on thermal performance.

2. Experimental Apparatus and Data Analyses

This section describes the experimental setup, nanofluid preparation procedure, heat transfer analysis, and the physical mechanisms associated with ultrasonic excitation and MWCNT nanofluids.

2.1. Experimental setup

The investigation was conducted inside a custom constructed air flow channel with dimensions of 200 cm × 35 cm × 35 cm. A remotely controlled blower fan governed the air circulation throughout experiments, enabling systematic variation of flow conditions. A schematic depiction of the configuration and its instrumentation is presented in Fig. 1.

An aluminum FTHX (250 mm × 130 mm) acted as the core component of the test section. Ultrasonic vibration was introduced through a 40 kHz piezoelectric transducer (Hesentec HS 8SH 3840); it was coupled with a PCB driver and an ultrasonic generator and provided a stable 50 W excitation power. This power corresponds to the ultrasonic excitation applied to the heat exchanger during experiments. The driving current of the transducer was maintained at 0.2 A. The transducer was located on a metal belt with a width of 20 mm and a thickness of 3 mm to ensure secure mechanical contact with the radiator during operation. Each configuration was examined under two regimes, ultrasonic activation and non-excited reference, to assess the influence of vibration on the thermal efficiency of the radiator.

Temperature and flow measurements inside the channel were captured by a network of high-precision sensors and meters. Three Maxim thermal probes (±0.0625 °C) were positioned near the liquid inlet and outlet and within the airstream. The coolant temperature spanned from 10 °C at entry to nearly 20 °C at discharge, whereas air temperatures varied between 25 °C and 45 °C. Flow diagnostics were handled by a Testo 400 airflow meter (range 0–10 m/s, accuracy ±0.04 m/s) and a Nixon NT5 volumetric flow meter (1.2–10 L/min, accuracy ±5 %). Water circulation was maintained by a Lauda Alpha RA8 refrigerated unit, operating from –25 °C to +100 °C with ±0.05 °C stability.

To acquire and store sensor data, a purpose-built control module transmitted signals to a computer for subsequent analysis. Supplementary details of each subsystem are documented in reference [19]. For clarity, Table 1 summarizes the principal technical specifications of the employed instrumentation.

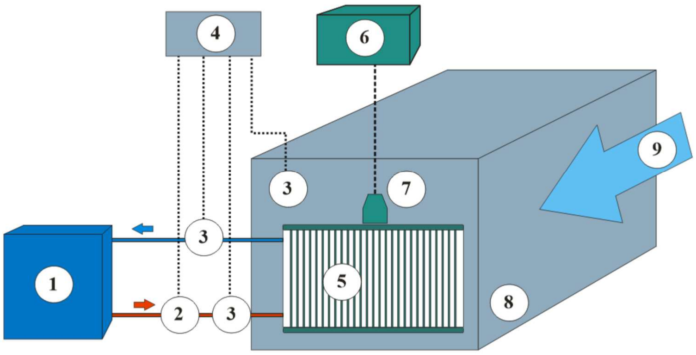

1	Refrigerated Circulator	6	Ultrasonic generator
2	Flowmeter	7	Piezoelectric transducer
3	Temperature Sensor	8	Air channel
4	Data acquisition unit	9	Air flow
5	Finned tube heat exchanger		

Fig. 1. The schematic of experimental setup.

Table 1. Summary of measurement and control equipment.

Instrument/ Component	Model & Manufacturer	Measurement Range	Precision/ Accuracy	Purpose
Thermal Sensors	Maxim Integrated Co.	−55 °C – +125 °C	± 0.0625 °C	Liquid & air temperatures
Air Velocity Meter	Testo 400	0 – 10 m/s	± 0.04 m/s	Air velocity measurement
Refrigerated Circulator	Lauda Alpha RA8	−25 °C – +100 °C	± 0.05 °C	Coolant temperature & flow regulation
Liquid Flow Meter	Nixon NT5	0.5– 5 l/min	± 5 %	Volumetric flow rate
Heat Exchanger	Aluminum radiator	250 mm × 130 mm	–	Test section component

The assessment concentrated on variations in outlet water temperature as the primary indicator of ultrasonic effectiveness. This parameter directly reflects the thermal response of the working fluid and the heat transfer enhancement caused by ultrasonic vibration.

2.2. Nanofluid preparation and stabilization

Multi-Walled Carbon Nanotubes (MWCNTs) are recognized for their superior thermal conductivity and low propensity for sedimentation, characteristics critical for the objectives of this investigation [23]. Specifically, MWCNTs with a purity of ≥95%, an average diameter ranging from 20 to 30 nm, and an average length of 5–10 µm were procured. Their solid, black form and a specific surface area between 32–40 m^2/g were also confirmed. The thermal conductivity of these MWCNTs is approximately 300 W/m.K, with a density of 2.1 g/cm^3 (or 2100 kg/m^3). Additionally, deionized water served as the base fluid for this study. The nanofluid was prepared using the two-step method, a widely adopted technique in the field for achieving stable colloidal suspensions [24, 25]. Initially, the precise mass of the MWCNT nanopowder was measured using a precision balance with an accuracy of 0.0001 g. The nanoparticles were then dispersed in deionized water using a semi-industrial ultrasonic homogenizer (UP 1200, Ultrasonic Technology Development Co., Iran) operating at a power of 1200 W and a frequency of 20 kHz. The sonication process was performed to promote uniform nanoparticle dispersion and reduce agglomeration. To minimize sedimentation effects and maintain nanofluid stability, the prepared suspension was used within two hours after the sonication process.

To accurately represent the thermal behavior of the nanofluid, several effective thermophysical properties were calculated based on the volume fraction (ϕ) of the MWCNT nanoparticles. These calculations were performed using established correlations found in the literature, ensuring a rigorous scientific approach. The effective density (ρ_{eff}) and specific heat capacity (c_{eff}) of the nanofluid were determined using standard mixing rules, as detailed in references [24, 25]. The effective viscosity (μ_{eff}) was computed employing the Brinkman correlation, a widely accepted model for estimating the viscosity of particle suspensions [26, 27]. Additionally, the thermal conductivity of the nanofluid (k_{eff}) was estimated via the Maxwell model, which provides a theoretical basis for predicting the effective thermal conductivity of composite materials [28].

2.3. Nusselt number definition, uncertainty analysis, and validation

The Nusselt number (Nu) represents the ratio between convective and conductive heat transfer at the boundary:

$$Nu = \frac{hD}{k_{eff}} \tag{1}$$

In this context, h represents the convective heat transfer coefficient, D is the tube diameter, and k_{eff} is the effective thermal conductivity of the nanofluid. The coefficient h itself is derived from the heat transfer rate (Q) over the surface area (A) and the bulk temperature difference (ΔT_{bulk}):

$$h = \frac{Q}{A\,\Delta T_{bulk}} \tag{2}$$

The bulk temperature difference ΔT_{bulk} is achieved using the Log Mean Temperature Difference (LMTD) method [29]:

$$\Delta T_{bulk} = \frac{T_i - T_o}{\ln\left(\dfrac{T_i - T_w}{T_o - T_w}\right)} \tag{3}$$

Here, T_i and T_o are the inlet and outlet temperatures of the nanofluid, respectively, measured by internal sensors. T_w is the measured wall temperature of the radiator tube. The experimental setup incorporated a controlled laboratory air conditioning duct (see Fig. 2) to maintain a constant radiator surface temperature (T_w). This system ensured precise temperature regulation (±0.1 °C) of the air flowing over the radiator, thus stabilizing T_w.

The Reynolds number (Re), which characterizes the flow regime, was computed as:

$$\mathrm{Re} = \frac{\rho V}{\nu} \tag{4}$$

where ρ is the fluid density, V is the flow velocity, D is the tube diameter, and ν is the kinematic viscosity.

An uncertainty analysis was conducted following the procedure proposed by Moffat [30]. The uncertainties associated with the primary measured variables, including temperature, liquid flow rate, and air velocity, were propagated through the governing equations used to calculate the heat transfer rate and Nusselt number. Based on the uncertainty propagation analysis, the maximum uncertainties were estimated to be ±2.6% for the heat transfer rate and ±3.4% for the Nusselt number. These values indicate that the experimental measurements and derived thermal parameters remain within acceptable engineering accuracy limits. Furthermore, as confirmed by Amiri Delouei et al. [31], validation against the Dittus–Boelter correlation [32] demonstrated reasonable conformity, ensuring reliability of the obtained data within accepted engineering bounds.

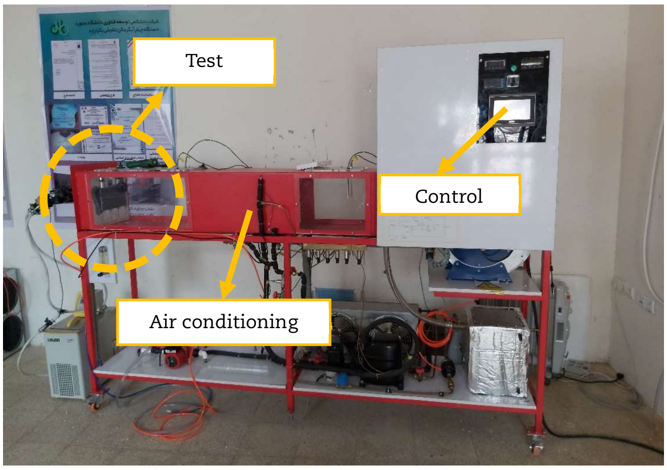

Fig. 2. Controlled laboratory air conditioning duct and experimental setup.

2.4. Physical mechanisms of heat transfer enhancement under ultrasonic excitation and MWCNT nanofluids

Ultrasonic-assisted heat transfer enhancement has been investigated for several decades, and a number of mechanisms have been proposed to explain the observed thermal improvements [33, 34]. When ultrasonic waves propagate through a liquid, several phenomena may occur, including acoustic cavitation, acoustic streaming, progressive heating, and nebulization. Among these mechanisms, acoustic cavitation and acoustic streaming are generally considered the dominant effects under the operating conditions commonly used in heat transfer applications [33].

Acoustic cavitation refers to the formation, growth, oscillation, and collapse of microscopic vapor or gas bubbles within the liquid. The phenomenon occurs when local pressure fluctuations generated by ultrasonic waves reduce the pressure below the vapor pressure of the fluid. The collapse of these bubbles near solid surfaces disturbs both the hydrodynamic and thermal boundary layers. This process promotes local mixing and micro-scale turbulence, which increases the convective heat transfer coefficient and reduces thermal resistance at the fluid–solid interface [35].

Acoustic streaming describes the steady fluid motion induced by the dissipation of acoustic energy within the liquid. This mechanism generates additional circulation and mixing, which can enhance momentum and energy transport [36]. Previous studies have shown that acoustic streaming contributes to improved convection by increasing fluid motion near heat transfer surfaces [37].

In finned-tube heat exchangers, ultrasonic excitation can influence both the internal and external heat transfer processes. On the liquid side, cavitation-induced microturbulence improves thermal transport between the nanofluid and the tube wall. On the air side, mechanical vibration of the heat exchanger structure can disturb the boundary layer adjacent to the fin surfaces, thereby increasing the external convective heat transfer coefficient [19]. The presence of MWCNT nanoparticles further enhances thermal performance. Carbon nanotubes possess high intrinsic thermal conductivity and can increase the effective thermal conductivity of the base fluid. In addition, nanoparticles may act as nucleation sites for bubble formation, which can intensify cavitation activity and strengthen the associated mixing effects. Consequently, the combined use of ultrasonic excitation and MWCNT nanofluids can produce a greater enhancement than either technique applied independently [19]. The effectiveness of ultrasonic enhancement is influenced by operating conditions such as nanoparticle concentration, fluid temperature, and flow velocity. Increasing nanoparticle concentration generally promotes cavitation activity and improves thermal transport. In contrast, higher temperatures may reduce dissolved gas content and alter bubble dynamics, which can weaken cavitation intensity. Similarly, at high flow velocities, the contribution of ultrasonic-induced mixing may become less pronounced because forced convection already provides substantial fluid mixing [19].

3. Model Specification

The input variables selected for modeling with the ANFIS network encompass key operational and material parameters, including air velocity, inlet temperature, nanoparticle concentration, and ultrasonic power. These variables represent the primary factors that influence the thermal and fluid dynamics within the system [38, 39]. The network's output variables, on the other hand, are critical performance indicators, including the outlet temperature, heat transfer rate, and the Nusselt number, which collectively reflect the efficiency and effectiveness of the heat transfer process. By incorporating these inputs and outputs, the ANFIS model is capable of capturing complex nonlinear relationships and interactions among the variables, enabling accurate prediction and optimization of system behavior under various operating conditions. This approach not only facilitates a deeper understanding of the underlying physical mechanisms but also provides a powerful tool for designing and controlling advanced thermal systems involving nanoparticles and ultrasonic enhancement techniques. Utilizing available experimental data to estimate unmeasured values minimizes the need for additional experiments by employing modeling and predictive techniques. In this study, the ANFIS models were developed and optimized using both the GA and PSO methods. The complete dataset consisted of 108 samples and was split into two subsets. 81 samples (75%) were used for training and 27 samples (25%) for testing. To ensure a robust assessment, the testing and training datasets were randomly and independently selected from the original dataset.

3.1. Adaptive neuro-fuzzy inference system (ANFIS)

In the ANFIS structure, the Takagi-Sugeno type fuzzy inference system is represented as a multilayer network. This network usually includes input layers, fuzzification, fuzzy rules, normalization, defuzzification, and output layers. Fuzzy membership functions, often chosen as Gaussian or bell functions, play an important role in converting deterministic inputs into fuzzy values. The parameters of these functions, as well as the parameters of the consequent part of the fuzzy rules, are automatically adjusted during the training process of the network [21, 40].

One of the outstanding features of ANFIS is the use of a hybrid learning algorithm that uses the least squares method to estimate the result parameters and the gradient descent method to update the initial parameters (membership functions). This approach increases the convergence speed and improves the accuracy of the model. Due to these advantages, the ANFIS network has been widely used in various fields such as forecasting, control, system identification, financial problems, and investment portfolio optimization. The ANFIS network is built based on the Takagi-Sugeno (TS) fuzzy inference system and usually consists of six layers. For simplicity, let us assume that the system has two inputs, x and y, and two fuzzy rules:

Rule 1: If x is a member of A_1 and y is a member of B_1, then: $f_1 = p_1 x + q_1 y + r_1$

Rule 2: If x is a member of A_2 and y is a member of B_2, then: $f_2 = p_2 x + q_2 y + r_2$

- First layer (Input layer): This layer is only responsible for transferring input values to the next layer and does not perform any operations:

$$O_i^{(1)} = x_i \tag{5}$$

- Second layer (Fuzzification layer): In this layer, inputs are converted into membership degrees using fuzzy membership functions. The output of each neuron is equal to the value of the membership function:

$$O_i^{(2)} = \mu_{A_i}(x) \text{or} \, \mu_{B_i}(y) \tag{6}$$

If the Gaussian membership function is used as an example, it is expressed as follows:

$$\mu(x) = \exp\left(-\frac{(x-c)^2}{2\sigma^2}\right) \tag{7}$$

The parameters c and σ are the premise parameters.

- Layer 3: Fuzzy Rule Layer: Each neuron corresponds to a fuzzy rule and calculates the Firing Strength of the rule:

$$O_i^{(3)} = w_i = \mu_{A_i}(x) \times \mu_{B_i}(y) \tag{8}$$

- Layer 4: Normalization Layer
  At this stage, the firing strength associated with each rule is normalized to determine its relative contribution:

$$O_i^{(4)} = \bar{w}_i = \frac{w_i}{\sum_j w_j} \tag{9}$$

- Layer 5: Defuzzification Layer
  Each neuron multiplies the normalized output of the rule by the resulting linear function:

$$O_i^{(5)} = \bar{w}_i f_i = \bar{w}_i (p_i x + q_i y + r_i) \tag{10}$$

The parameters p_i, q_i, r_i are the consequent parameters.

- Layer 6: Output Layer
  Finally, the output of the entire network is obtained from the sum of the outputs of the previous layer:

$$O_i^{(6)} = \sum_i \bar{w}_i f_i \tag{11}$$

ANFIS is a hybrid intelligent model that aims to simultaneously utilize the capabilities of fuzzy logic and artificial neural networks. Fuzzy logic has a high ability to model uncertainty, ambiguity, and human linguistic knowledge, while artificial neural networks are known for their learning power, generalizability, and data adaptation. By combining these two approaches, ANFIS provides a flexible and efficient model for approximating nonlinear functions and solving complex problems.

ANFIS employs a hybrid learning algorithm in which the consequent parameters are estimated using the Least Squares method, while the parameters of the membership functions are adjusted through Gradient Descent. The combination of these two learning approaches leads to faster convergence and improved network accuracy.

By representing the fuzzy system as a multilayer neural network, the ANFIS network provides the ability to automatically learn fuzzy rules and membership functions and is a powerful tool for modeling nonlinear and complex systems. The structure of the ANFIS network is shown in Fig. 3.

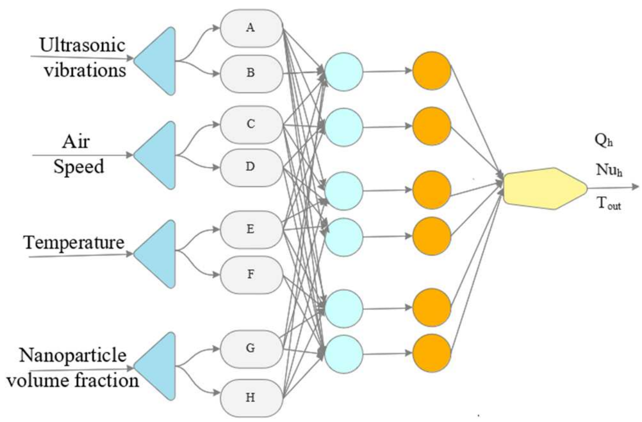

Fig. 3. The configuration of the ANFIS network employed in this study.

Table 2 summarizes the ANFIS configuration used in this study, including the fuzzy inference system (FIS) type, membership function (MF) type, and the optimization methods, namely backpropagation and the hybrid approach.
As shown in Table 2, the maximum value of coefficient of determination (R^2) is 0.842, which is lower than the desired value of 1.0. To improve prediction accuracy, the ANFIS model can be further optimized using GA and PSO algorithms.

The modeling dataset consisted of 108 experimental data points obtained under different operating conditions. Of these data, 81 samples were used for training and 27 samples were reserved for testing. The dataset size is comparable to those employed in several ANFIS-based thermal engineering studies reported in the literature [7, 11]. The testing dataset was not used during the training process and was reserved exclusively for model evaluation.

3.2. Genetic algorithm (GA)

GA is a metaheuristic and evolutionary optimization method first introduced by Holland in 1975 [41]. Inspired by the natural evolution process, this algorithm starts its search from an initial population of random solutions. Each solution is represented as a string or chromosome, which contains a set of genes. The quality of each chromosome is assessed through a fitness function.

In each iteration, referred to as a generation, genetic operators such as selection, crossover, and mutation are applied. The selection operator selects the most suitable chromosomes to produce the next generation. In the crossover operator, the genetic information of the parents is combined and new offspring are created. The mutation operator also prevents premature convergence by making small and random changes in the genes. By repeating this process in successive generations, the GA gradually guides the population towards the optimal or near-optimal response and usually stops after reaching a certain number of iterations or fulfilling a stopping criterion [42, 43].

3.3. Particle swarm optimization (PSO) algorithm

PSO is inspired by the collective behavior observed in nature, such as bird flocks and fish schools during food searching, and is therefore considered a population-based social search method. In this technique, each particle corresponds to a candidate solution and mimics the movement of an individual within a coordinated group. The quality of every particle is assessed through an objective (fitness) function. By sharing information within the swarm, particles cooperatively move toward improved solutions, which generally makes the method more efficient than isolated search strategies.

At the start of the process, particles are assigned random initial positions and velocities. During successive iterations, the position of each particle is updated using its own best historical position and the best position identified by the swarm. This information-sharing mechanism gradually directs the population toward the global optimum. The velocity and position updates of each particle are determined by Eqs. (12) and (13):

$$V_i(t+1) = \omega V_i(t) + c_1 \times rand_1\left(pbest_i(t) - x_i(t)\right) + c_2 \times rand_2\left(gbest_i(t) - x_i(t)\right) \tag{12}$$

$$x_i(t+1) = x_i(t) + V_i(t+1) \tag{13}$$

here, '*gbest*' denotes the best solution identified by the entire swarm, whereas '*pbest*' indicates the best position previously achieved by an individual particle. The variable t represents the iteration number.

Table 2. ANFIS configuration employed in this study.

No.	FIS	Input MFs	Number of MFs	Optimum method	R^2 (average)		
					T_{out}	Q	$N_{u_{LMTD}}$
1	Genfis1	Gaussmf	3	Backpropagation	0.563	0.599	0.607
			4		0.589	0.603	0.611
			5		0.612	0.614	0.618
			3	Hybrid	0.671	0.608	0.622
			4		0.685	0.611	0.623
			5		0.702	0.699	0.634
		gbellf	3	Backpropagation	0.603	0.587	0.633
			4		0.621	0.599	0.634
			5		0.640	0.601	0.654
			3	Hybrid	0.637	0.620	0.656
			4		0.640	0.622	0.666
			5		0.692	0.622	0.673
2	Genfis2	Range of fluence	0.1	Backpropagation	0.880	0.799	0.810
			0.3		0.881	0.808	0.812
			0.5		0.870	0.805	0.815
			0.1	Hybrid	0.850	0.803	0.844
			0.3		0.891	0.806	0.856
			0.5		0.891	0.805	0.851
3	Genfis3	Number of clusters	5	Backpropagation	0.775	0.790	0.803
			10		0.784	0.792	0.806
			15		0.791	0.791	0.806
			5	Hybrid	0.796	0.801	0.831
			10		0.796	0.802	0.832
			15		0.793	0.802	0.842

The coefficients c_1 and c_2 are acceleration constants that control the influence of individual experience (cognitive component) and group experience (social component), typically ranging from 0 to 2. The random terms 'rand$_1$' and 'rand$_2$' are uniformly distributed between 0 and 1. The inertia weight ω, usually selected between 0 and 1, is often decreased gradually to balance exploration and exploitation during the search.

When PSO is applied to optimize ANFIS, the adjustable parameters generally include parameters of 'genfis 1', '2' and '3'. The procedure begins by randomly generating N position vectors X_i, where N is the swarm size. In practice, the population size is commonly chosen to be about four to five times the number of decision variables in the optimization problem [6, 44, 45].

Figure 4 illustrates the structure of the ANFIS optimization model using GA and PSO algorithms.

4. Results and Discussion

Here, variations in outlet temperature (T_o), heat transfer rate (Q), and Nusselt number (Nu_{LMTD}) at different inlet temperatures (T_i), air velocity, ultrasonic powers (UP), and nanofluid concentrations (Φ_w) were investigated. The experimental data were used to validate the results predicted by the ANFIS-GA and ANFIS-PSO models.

4.1. Outlet temperature

The outlet temperature in heat exchangers is considered one of the most critical operating parameters, as it directly affects heat transfer efficiency, energy consumption, and overall process performance. Proper control of this temperature plays a significant role in achieving desired thermal conditions, improving final product quality, and minimizing energy losses. In many industrial processes, the primary purpose of using a heat exchanger is to bring a fluid to a specified temperature for subsequent stages such as cooling, chemical reactions, distillation, evaporation, or drying. Therefore, any deviation from the desired outlet temperature can lead to reduced efficiency, lower product purity, or even unsafe operating conditions.

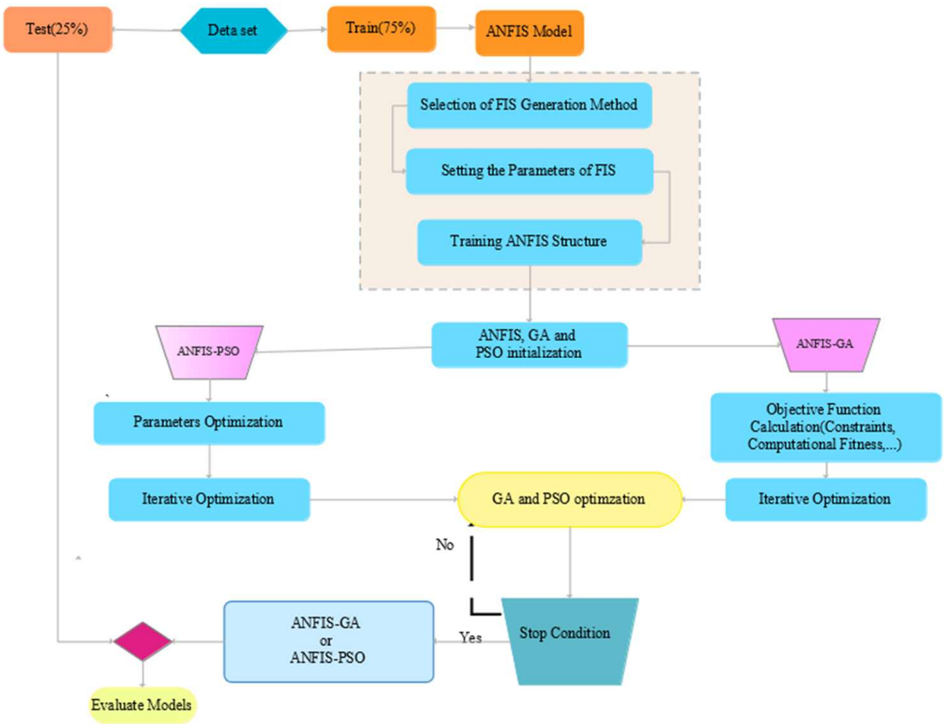

Fig. 4. Flowchart of the ANFIS optimization model based on GA and PSO algorithms.

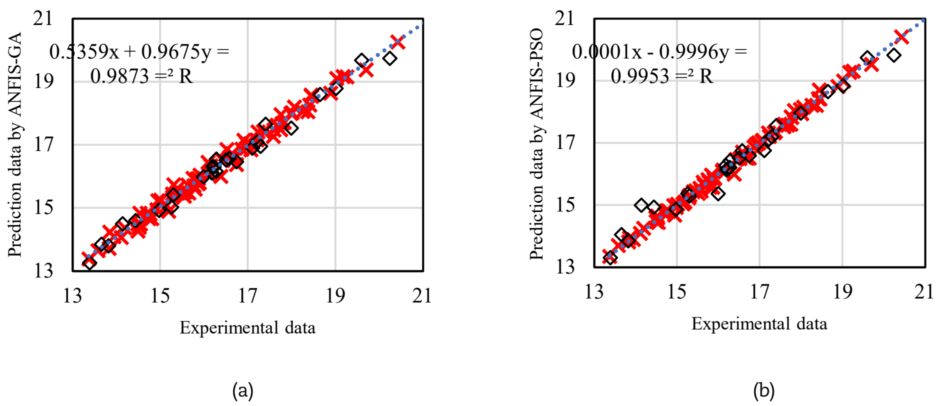

Fig. 5. Comparison of experimental data and predicted data of outlet temperature for (a) ANFIS-GA and (b) ANFIS-PSO.

In summary, the outlet temperature of a heat exchanger is not merely a simple measurable variable, but a strategic indicator for process control, energy optimization, product quality assurance, and the maintenance of operational safety in industrial applications. Figures 5(a) and 5(b) illustrate the comparison between the T_{out} experimental values and the outputs predicted by the ANFIS-GA and ANFIS-PSO models, respectively. The coefficient of determination (R^2) was employed to evaluate how well the predicted results matched the target data and to quantify the explained variance. The obtained results demonstrate a strong agreement between model predictions and measured values. Moreover, the training phase of the models showed high performance, with the R^2 value reaching 0.98, indicating excellent predictive capability.

Figure 6 compares the prediction errors of different ANFIS models trained with GA and PSO algorithms. The blue and orange boxes represent the training and testing errors of the ANFIS-GA model, respectively, while the gray and yellow boxes correspond to the ANFIS-PSO model.

Regarding Fig. 6, the prediction errors of both ANFIS-GA and ANFIS-PSO models are generally centered around zero, indicating good agreement between the predicted and experimental outlet temperatures. The ANFIS-PSO model exhibits a smaller median error and a narrower interquartile range, suggesting a more compact distribution of temperature prediction errors. Although several outliers are observed in the testing dataset, most prediction errors remain within a relatively narrow range. These results indicate that both optimization approaches provide reliable temperature predictions, while the ANFIS-PSO model exhibits slightly lower error dispersion for this output parameter.

4.2. Heat transfer rate

The heat transfer rate predictions obtained from the optimized ANFIS models, using both GA and PSO approaches, are presented in Fig. 7. The figure compares the predicted values with the experimental data, illustrating the accuracy of the models in capturing the thermal behavior of the system. It can be observed that both ANFIS-GA and ANFIS-PSO closely follow the experimental trend, with minor deviations at specific sample points. Among the two, the PSO-optimized model exhibits slightly higher agreement with the experimental measurements, indicating its superior capability in modeling complex nonlinear interactions in the system. These results demonstrate the effectiveness of the ANFIS approach combined with evolutionary optimization techniques for accurate prediction of heat transfer performance in nanoparticle-enhanced thermal systems.

4.3. Nusselt number

The accuracy of the proposed models and the agreement between experimental and predicted Nusselt numbers are evaluated. A dataset of 108 laboratory measurements is used to assess the modeling and optimization performance of ANFIS-GA and ANFIS-PSO approaches. The results demonstrate strong predictive capability and effective optimization performance for both methods. Figure 8 compares the Nusselt number (Nu) values predicted by the ANFIS-GA and ANFIS-PSO models with the experimental data.

4.4. Comparison of ANFIS-GA and ANFIS-PSO models

A sensitivity analysis was performed using the optimized ANFIS-GA and ANFIS-PSO models to evaluate the relative influence of the input variables on the predicted thermal responses. The input variables included inlet temperature, air velocity, nanoparticle concentration, and ultrasonic power. Each parameter was varied within its experimental range while the corresponding changes in outlet temperature, heat transfer rate, and Nusselt number were monitored. The relative importance of each parameter was quantified using its normalized contribution to the model outputs. The resulting sensitivity percentages indicate the extent to which each operating parameter affects the thermal performance indicators.

The sensitivity analysis presented in Fig. 9 offers a detailed look at how output parameters of To, Q, and Nusselt number change with various input variables (air velocity, T_i, Φ_w, and UP) of the system using ANFIS-GA and ANFIS-PSO models. In Fig. 9(a), the outlet temperature (T_o) exhibits a balanced sensitivity to the input parameters of T_i, Φ_w, and UP.

Notably, T_i, Φ_w, and UP are identified as the most critical factors, collectively accounting for approximately 88% of the model's overall sensitivity for To. In this specific case, air velocity has the lowest impact, accounting for only about 12% of the total importance.

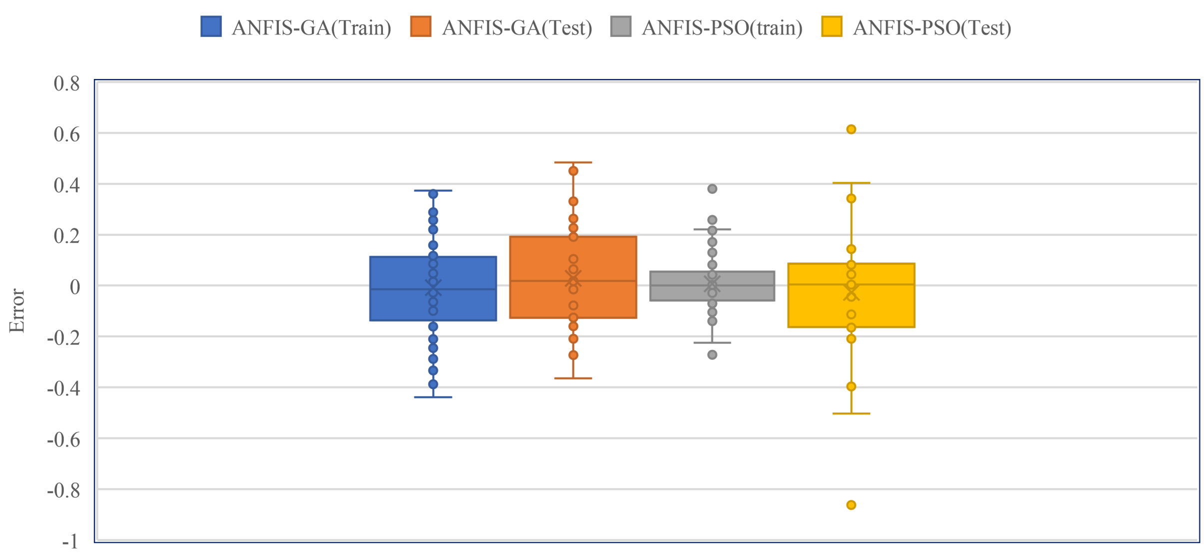

Fig 6. Comparison of temperature prediction errors for ANFIS models trained with GA and PSO algorithms (training and testing sets).

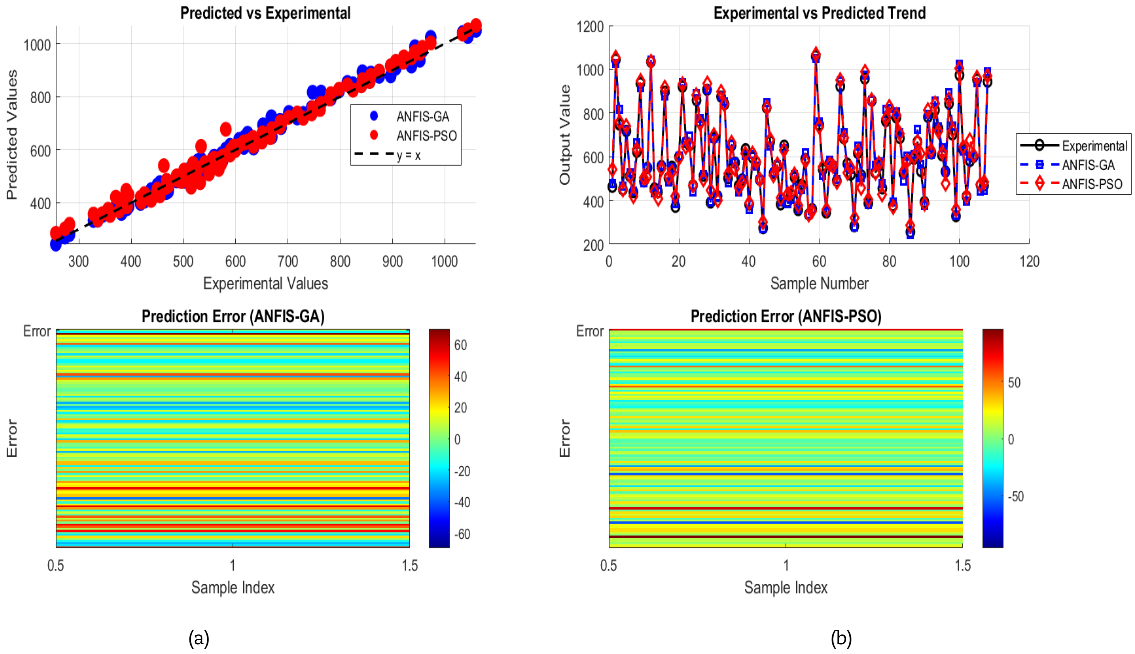

Fig. 7. Performance comparison of optimized ANFIS models with (a) GA and (b) PSO approaches.

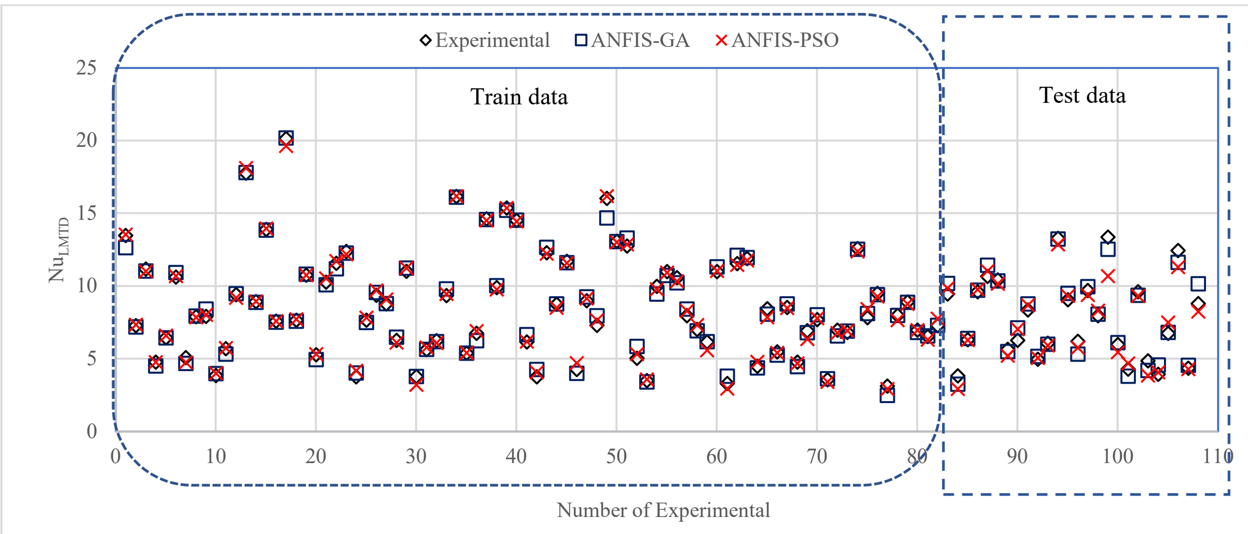

Fig. 8. Comparison of the ANFIS-GA and ANFIS-PSO model predictions with experimental measurements for the FTHX.

When analyzing the heat transfer rate (Fig. 9(b)), Φ_w becomes the dominant variable with an importance of over 43%, followed closely by UP at roughly 37%. Interestingly, the inlet temperature plays a negligible role in determining the heat transfer rate, showing a sensitivity of less than 5%.

Finally, for the Nusselt Number (Fig. 9(c)), Φ_w remains the most influential parameter at approximately 40%, while UP maintains a secondary importance of around 27%. Across all three parameters, the outputs obtained from the ANFIS-GA and ANFIS-PSO algorithms are remarkably consistent, suggesting that both optimization methods are equally reliable in predicting the sensitivity of these thermal outputs.

A strong correlation exists between the experimental measurements and the predictions from both the ANFIS-GA and ANFIS-PSO models. A close agreement is observed between the model outputs and the experimental data, confirming that both approaches can reliably represent the system behavior. Table 3 presents a comprehensive statistical evaluation of the developed models using R^2, MSE, RMSE, and MAE for the training, testing, and overall datasets.

Also, a comparison of Tables 2 and 3 indicates that integrating ANFIS with GA and PSO enhances the prediction of output parameters. The hybrid models show superior performance relative to the standalone ANFIS model.

The training and testing statistics are in good agreement for both ANFIS-GA and ANFIS-PSO models. For example, the ANFIS-GA model produced R^2 values of 0.988 and 0.989 for the training and testing datasets of outlet temperature, respectively. Similar trends were observed for heat transfer rate and Nusselt number. The relatively small differences between the training and testing performance metrics indicate satisfactory generalization capability and suggest that significant overfitting was not observed. Based on the higher R^2 values and lower error metrics, the ANFIS-GA model exhibits slightly better overall performance than the ANFIS-PSO model.

Table 3. Statistical evaluation of the developed models in this study.

		ANFIS-GA			ANFIS-PSO		
		Train	Test	Overall	Train	Test	Overall
	Number of data	81	27	108	81	27	108
R^2	T	0.988	0.989	0.988	0.99	0.98	0.988
	Q	0.989	0.989	0.989	0.985	0.979	0.984
	$N_{u_{LMTD}}$	0.987	0.963	0.981	0.986	0.936	0.974
MSE	T	0.032	0.045	0.035	0.012	0.077	0.028
	Q	376.079	818.245	486.621	483.199	985.062	608.665
	$N_{u_{LMTD}}$	0.113	0.293	0.158	0.057	0.516	0.172
MAE	T	0.146	0.169	0.151	0.078	0.189	0.106
	Q	14.784	24.111	17.116	16.524	22.317	17.972
	$N_{u_{LMTD}}$	0.237	0.416	0.282	0.185	0.507	0.265
RMSE	T	0.179	0.212	0.187	0.11	0.277	0.167
	Q	19.393	28.605	22.059	21.982	31.386	24.671
	$N_{u_{LMTD}}$	0.336	0.541	0.397	0.239	0.718	0.415

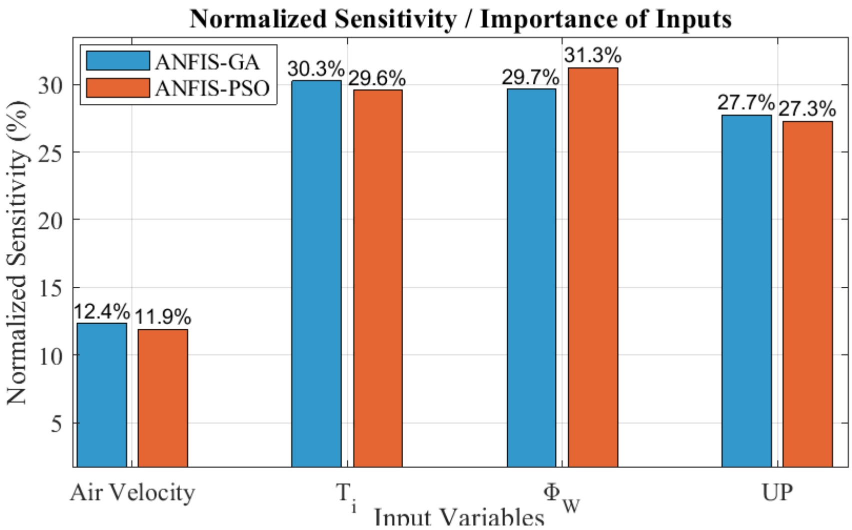

(a)

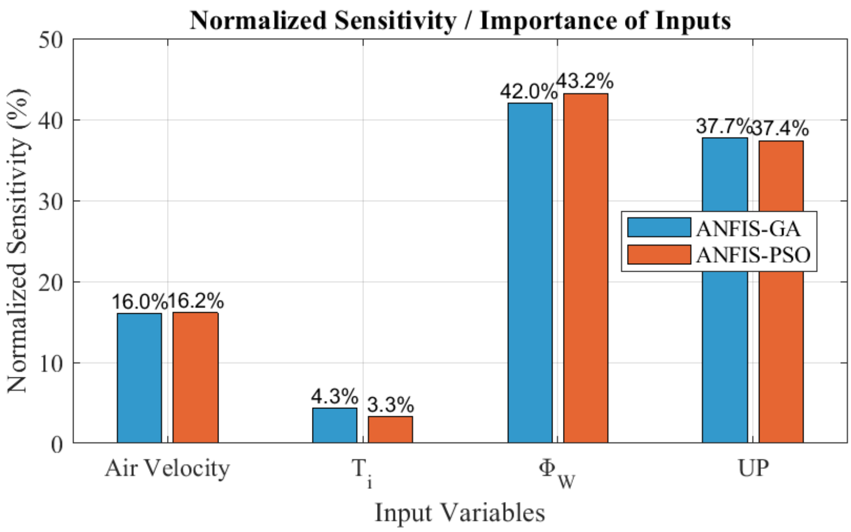

(b)

Fig. 9. Sensitivity analysis of output parameters of (a) T_o, (b) Q, and (c) Nu_{LMTD} under different input parameters (air velocity, T_i, Φ_w, and UP).

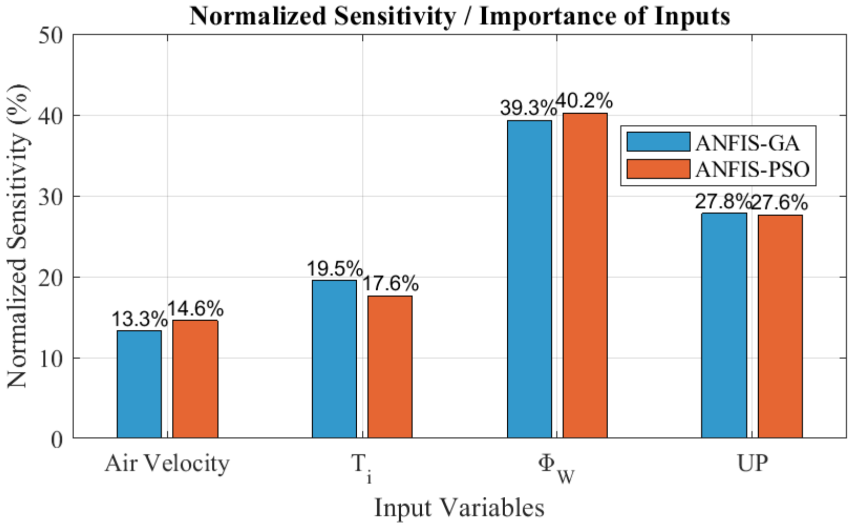

(c)

Fig. 9. Continued.

5. Industrial Applicability and Limitations

The proposed ANFIS-based framework demonstrates strong potential for application in advanced industrial thermal systems, including compact heat exchangers, Ventilation, and Air Conditioning (HVAC) systems, electronic cooling devices, and energy recovery processes. The developed intelligent model can accurately predict thermal performance under different operating conditions, thereby reducing the need for extensive experimental measurements, computational effort, and associated costs. Furthermore, the combination of ultrasonic excitation and MWCNT nanofluids resulted in considerable heat transfer enhancement, which may improve the thermal efficiency of industrial heat transfer equipment.

Nevertheless, several practical limitations should be considered for large-scale industrial implementation. Scaling the laboratory system to industrial applications may increase the complexity of flow management, ultrasonic energy consumption, and system maintenance requirements. In addition, the preparation and stabilization of nanofluids may increase operational costs compared with conventional working fluids. Another important limitation is the long-term stability of MWCNT nanofluids, since nanoparticle agglomeration and sedimentation during prolonged operation may reduce thermal performance and affect system reliability. Therefore, further investigations under industrial-scale and long-duration operating conditions are necessary to evaluate the economic feasibility, durability, and long-term operational stability of the proposed enhancement method.

6. Conclusion

An ANFIS-based modeling framework optimized using GA and PSO algorithms was developed to predict the thermal performance of an ultrasonically assisted finned-tube heat exchanger operating with MWCNT nanofluids. Based on the experimental and modeling results, the following conclusions can be drawn:

- Both ANFIS-GA and ANFIS-PSO models successfully predicted outlet temperature, heat transfer rate, and Nusselt number with high accuracy, showing strong agreement with the experimental measurements.
- Overall statistical analyses indicate that the ANFIS-GA model provides slightly better overall predictive performance and robustness than the ANFIS-PSO model, although ANFIS-PSO demonstrated lower error dispersion in some individual prediction cases.
- Sensitivity analysis revealed that inlet temperature, nanoparticle concentration, and ultrasonic power were the dominant parameters influencing thermal performance, whereas air velocity had a comparatively smaller effect.
- The combined application of ultrasonic excitation and MWCNT nanofluids enhanced the heat transfer characteristics of the finned-tube heat exchanger, demonstrating the effectiveness of this thermal enhancement technique.
- The proposed ANFIS-GA framework provides a practical tool for predicting thermal performance under different operating conditions and can reduce the need for extensive experimental testing in the design and analysis of enhanced heat exchanger systems.

Future studies may focus on larger datasets, additional nanofluid formulations, and industrial-scale operating conditions to further evaluate the applicability of the proposed methodology.

Author Contributions

A. Amiri Delouei is the single author who was responsible for overall contributions.

Acknowledgments

Not applicable.

Conflict of Interest

The author declared no potential conflicts of interest concerning the research, authorship, and publication of this article.

Funding

The author received no financial support for the research, authorship, and publication of this article.

Data Availability Statements

The datasets generated and/or analyzed during the current study are available from the corresponding author on reasonable request.

References

[1] Zhong, J., Wang, Y., Li, M., Pei, G., Tang, S., Rong, J., Xu, C., Kang, L., Deng, J., Shan, S., Zhou, L., Heat transfer characteristics of the fin-tube three-fluid heat exchanger in cold warehouse with cold storage, *Energy*, 347, 2026, 140362.
[2] Zhang, D., Ji, L., Wang, W., Li, J., Zhao, S., Fan, Y., Liu, B., Performance analysis of a large-scale metal hydride reactor with a finned-tube heat exchanger, *Applied Thermal Engineering*, 280, 2025, 128423.
[3] Mohammadpour, A.A., Jafari, B., Hosseinzadeh, K., Thermal enhancement analysis of PCM-filled finned tube heat exchangers using metal foams in building HVAC systems, *Journal of Building Engineering*, 120, 2026, 115276.
[4] Rezaei, P., Moheghi, H.R., Amiri Delouei, A., Design and optimization of a spiral-tube instantaneous water heater using response surface methodology, *Water*, 15, 2023, 1458.
[5] Esfandyari, M., Sajjadi, H., Delouei, A.A., GMDH and RSM models for prediction of heat transfer parameters in an ultrasonic vibrating fin-and-tube heat exchanger, *International Journal of Heat and Fluid Flow*, 114, 2025, 109795.
[6] Esfandyari, M., Amiri Delouei, A., Jalali, A., Optimization of ultrasonic-excited double-pipe heat exchanger with machine learning and PSO, *International Communications in Heat and Mass Transfer*, 147, 2023, 106985.
[7] Mehrabi, M., Pesteei, S.M., Pashaee G., T., Modeling of heat transfer and fluid flow characteristics of helicoidal double-pipe heat exchangers using adaptive neuro-fuzzy inference system (ANFIS), *International Communications in Heat and Mass Transfer*, 38, 2011, 525–532.
[8] Barmavatu, P., Radhakrishnan, A., Pawar, S.R., Salve, S., Prasad, B.D., Heat transfer coefficient prediction and increase the effectiveness in fin-and-tube heat exchangers using machine learning approaches, *Journal of Thermal Science and Engineering Applications*, 17, 2025, 91001.
[9] Khan, J.S., Ahmad, I., Jadoon, U.K., Samad, A., Saghir, H., Kano, M., Caliskan, H., Artificial intelligence based prediction of optimum operating conditions of a plate and fin heat exchanger under uncertainty: a gray-box approach, *International Journal of Heat and Mass Transfer*, 217, 2023, 124653.
[10] Kunjuraman, S., Velusamy, B., Performance evaluation of shell and tube heat exchanger through ANN and ANFIS model for dye recovery from textile effluents, *Energy Sources, Part A: Recovery, Utilization, and Environmental Effects*, 43, 2021, 1600–1619.
[11] Gupta, A.K., Kumar, P., Sahoo, R.K., Sahu, A.K., Sarangi, S.K., Performance measurement of plate fin heat exchanger by exploration: ANN, ANFIS, GA, and SA, *Journal of Computational Design and Engineering*, 4, 2017, 60–68.
[12] Amiri Delouei, A., Sajjadi, H., Izadi, M., Mohebbi, R., The simultaneous effects of nanoparticles and ultrasonic vibration on inlet turbulent flow: an experimental study, *Applied Thermal Engineering*, 146, 2019.
[13] Trisaksri, V., Wongwises, S., Critical review of heat transfer characteristics of nanofluids, *Renewable and Sustainable Energy Reviews*, 11, 2007, 512–523.
[14] Alizadeh, A., Kriaa, K., Mohsen, A.M., Othayq, M.M., Al-Zahiwat, M.M., Sadeq, A.M., Rajab, H., Hajlaoui, K., Numerical and statistical analysis of hybrid nanofluid impact on finned shell and coil heat exchanger performance, *Journal of Engineering Research*, 2026.
[15] Amiri Delouei, A., Sajjadi, H., Mohebbi, R., Izadi, M., Experimental study on inlet turbulent flow under ultrasonic vibration: pressure drop and heat transfer enhancement, *Ultrasonics Sonochemistry*, 51, 2019.
[16] Amiri Delouei, A., Sajjadi, H., Ahmadi, G., Ultrasonic vibration technology to improve the thermal performance of CPU water-cooling systems: experimental investigation, *Water*, 14, 2022, 4000.
[17] Amiri Delouei, A., Naeimi, H., Sajjadi, H., Atashafrooz, M., Imanparast, M., Chamkha, A.J., An active approach to heat transfer enhancement in indirect heaters of city gate stations: an experimental modeling, *Applied Thermal Engineering*, 237, 2024, 121795.
[18] Hedeshi, M., Jalali, A., Arabkoohsar, A., Amiri Delouei, A., Nanofluid as the working fluid of an ultrasonic-assisted double-pipe counter-flow heat exchanger, *Journal of Thermal Analysis and Calorimetry*, 148, 2023, 8579–8591.
[19] Amiri, A., Atashafrooz, M., Sajjadi, H., Karimnejad, S., The thermal effects of multi-walled carbon nanotube concentration on an ultrasonic vibrating finned tube heat exchanger, *International Communications in Heat and Mass Transfer*, 135, 2022, 106098.
[20] Esfandyari, M., Esfandyari, M., Jafari, D., Prediction of thiophene removal from diesel using [BMIM][$AlCl_4$] in EDS process: GA-ANFIS and PSO-ANFIS modeling, *Petroleum Science and Technology*, 2018.
[21] Bekhradinassab, E., Esfandyari, M., Biodiesel production by iron oxide supported on light weight expanded clay aggregate (Fe_2O_3-f-LECA) catalyst: Box-Behnken design-based optimization and ANFIS modeling with GA and PSO, *Renewable Energy*, 251, 2025, 123466.
[22] Shamshirband, S., Hadipoor, M., Baghban, A., Mosavi, A., Bukor, J., Várkonyi-Kóczy, A.R., Developing an ANFIS-PSO model to predict mercury emissions in combustion flue gases, *Mathematics*, 7, 2019, 965.
[23] Taherian, H., Alvarado, J.L., Languri, E.M., Enhanced thermophysical properties of multiwalled carbon nanotubes based nanofluids. Part 2: experimental verification, *Renewable and Sustainable Energy Reviews*, 82, 2018, 4337–4344.
[24] Lee, J., Mudawar, I., Assessment of the effectiveness of nanofluids for single-phase and two-phase heat transfer in micro-channels, *International Journal of Heat and Mass Transfer*, 50, 2007, 452–463.
[25] Nazari, M., Ashouri, M., Kayhani, M.H., Tamayol, A., Experimental study of convective heat transfer of a nanofluid through a pipe filled with metal foam, *International Journal of Thermal Sciences*, 88, 2015, 33–39.
[26] Brinkman, H.C., The viscosity of concentrated suspensions and solutions, *Journal of Chemical Physics*, 20, 1952, 571.
[27] Halelfadl, S., Estellé, P., Aladag, B., Doner, N., Maré, T., Viscosity of carbon nanotubes water-based nanofluids: influence of concentration and temperature, *International Journal of Thermal Sciences*, 71, 2013, 111–117.
[28] Xue, Q.Z., Model for thermal conductivity of carbon nanotube-based composites, *Physica B: Condensed Matter*, 368, 2005, 302–307.
[29] Bezaatpour, M., Goharkhah, M., Convective heat transfer enhancement in a double pipe mini heat exchanger by magnetic field induced swirling flow, *Applied Thermal Engineering*, 167, 2020, 114801.
[30] Moffat, R.J., Describing the uncertainties in experimental results, *Experimental Thermal and Fluid Science*, 1, 1988, 3–17.
[31] Amiri Delouei, A., Sajjadi, H., Atashafrooz, M., Hesari, M., Ben Hamida, M.B., Arabkoohsar, A., Louvered fin-and-flat tube compact heat exchanger under ultrasonic excitation, *Fire*, 6, 2023, 13.
[32] Incropera, F.P., DeWitt, D.P., Bergman, T.L., Lavine, A.S., Fundamentals of Heat and Mass Transfer, John Wiley & Sons, New York, 2007.
[33] Legay, M., Gondrexon, N., Le Person, S., Boldo, P., Bontemps, A., Enhancement of heat transfer by ultrasound: review and recent advances, *International Journal of Chemical Engineering*, 2011, 670108.
[34] Laborde, J.-L., Hita, A., Caltagirone, J.-P., Gerard, A., Fluid dynamics phenomena induced by power ultrasounds, *Ultrasonics*, 38, 2000, 297–300.
[35] Neppiras, E.A., Acoustic cavitation series: part one: Acoustic cavitation: an introduction, *Ultrasonics*, 22, 1984, 25–28.
[36] Lighthill, S.J., Acoustic streaming, *Journal of Sound and Vibration*, 61, 1978, 391–418.
[37] Riley, N., Acoustic streaming, *Theoretical and Computational Fluid Dynamics*, 10, 1998, 349–356.
[38] Erdogan, B., Günes, A., Kılıç, İ., Yaman, O., Predicting thermal conductivity of nanoparticle-doped cutting fluid oils using feedforward artificial neural networks (FFANN), *Micromachines*, 16, 2025, 504.
[39] Behroozpour, A.A., Jafari, D., Esfandyari, M., Jafari, S.A., Prediction of the continuous cadmium removal efficiency from aqueous solution by the packed-bed column using GMDH and ANFIS models, *Desalination and Water Treatment*, 234, 2021, 91–101.
[40] Dolatabadi, M., Mehrabpour, M., Esfandyari, M., Alidadi, H., Davoudi, M., Modeling of simultaneous adsorption of dye and metal ion by sawdust from aqueous solution using of ANN and ANFIS, *Chemometrics and Intelligent Laboratory Systems*, 181, 2018, 72–78.

[41] Forrest, S., Genetic algorithms, *ACM Computing Surveys*, 28, 1996, 77–80.
[42] Mahrooghi, A., Lakzian, E., Optimization of Wells turbine performance using a hybrid artificial neural fuzzy inference system (ANFIS)-genetic algorithm (GA), *Ocean Engineering*, 226, 2021, 108861.
[43] Chen, W., Panahi, M., Pourghasemi, H.R., Performance evaluation of GIS-based new ensemble data mining techniques of adaptive neuro-fuzzy inference system (ANFIS) with genetic algorithm (GA), differential evolution (DE), and particle swarm optimization (PSO) for landslide spatial modelling, *Catena*, 157, 2017, 310–324.
[44] Alarifi, I.M., Nguyen, H.M., Naderi Bakhtiyari, A., Asadi, A., Feasibility of ANFIS-PSO and ANFIS-GA models in predicting thermophysical properties of Al_2O_3-MWCNT/oil hybrid nanofluid, *Materials*, 12, 2019, 3628.
[45] Bahiraei, M., Nazari, S., Safarzadeh, H., Modeling of energy efficiency for a solar still fitted with thermoelectric modules by ANFIS and PSO-enhanced neural network: a nanofluid application, *Powder Technology*, 385, 2021, 185–198.

ORCID iD

Amin Amiri Delouei https://orcid.org/0000-0001-7414-4195

How to cite this article: Amiri Delouei A. ANFIS-Based Modeling and Optimization of Heat Transfer in Ultrasonically Assisted Finned-Tube Heat Exchangers with MWCNT Nanofluids, *J. Appl. Comput. Mech.*, xx(x), 2026, 1-13. https://doi.org/10.22055/jacm.2026.49286.5867